Imaging of the Autonomic Nervous System in Cardiac Amyloidosis

16

Walter Noordzij, Andor W.J.M. Glaudemans, Riemer H.J.A. Slart, and Bouke P.C. Hazenberg

Contents

Abstract

Cardiac amyloidosis is a restrictive cardiomyopathy with potentially fatal consequences due to amyloid deposition in the myocardial tissue, but also to amyloid infiltration in the nerve conduction system. The prognosis is poor because of progressive cardiac disease. Early detection of cardiac involvement has become of major clinical interest, because its occurrence and severity limits the choice of treatment. The use of iodine-123 labelled metaiodobenzylguanidine

W. Noordzij, MD (✉) • A.W.J.M. Glaudemans, MD, PhD • R.H.J.A. Slart, MD, PhD
Department of Nuclear Medicine and Molecular Imaging, University of Groningen, University Medical Center Groningen, Hanzeplein 1, 9700 RB Groningen, The Netherlands
e-mail: w.noordzij@umcg.nl

B.P.C. Hazenberg, MD, PhD
Department of Rheumatology and Clinical Immunology, University of Groningen, University Medical Center Groningen, Hanzeplein 1, 9700 RB Groningen, The Netherlands

R.H.J.A. Slart et al. (eds.), *Autonomic Innervation of the Heart: Role of Molecular Imaging*, DOI 10.1007/978-3-662-45074-1_16

([^{123}I]-MIBG), a chemical modified analogue of norepinephrine, is well established in patients with heart failure and plays an important role in cardiac amyloidosis. [^{123}I]-MIBG is stored in vesicles in the sympathetic nerve terminals and is not catabolised like norepinephrine. Decreased heart-to-mediastinum ratios (HMR) on late planar images and increased wash-out rates indicate cardiac sympathetic denervation and are associated with poor prognosis. Single-photon emission computed tomography (SPECT) provides additional information and has advantages for evaluating abnormalities in regional distribution in the myocardium. However, inferior wall defects should be interpreted with caution.

Abbreviations

AA	Serum amyloid A protein type of amyloidosis
AF	Atrial fibrillation
AL	Immunoglobulin light chain type of amyloidosis
ANS	Autonomic nervous system
ATTR	Transthyretin type of amyloidosis
HMR	Heart-to-mediastinum ratio
HRV	Heart rate variability
LVEF	Left ventricular ejection fraction
MHED	Meta-hydroxy-ephedrine
MIBG	Meta-iodobenzylguanidine
MRI	Magnetic resonance imaging
SAP	Serum amyloid P component
SPECT	Single-photon emission computed tomography
TTE	Transthoracic echocardiography

16.1 Introduction

Cardiac amyloidosis is a rare disorder. Amyloidosis is caused by misfolded soluble serum proteins that are deposited extracellularly as insoluble amyloid fibrils throughout the body. All major types of systemic amyloidosis may display cardiac involvement. About 50 % of all amyloidosis patients experience some cardiac manifestations related to the disease. The prevalence of this cardiac involvement varies widely among the different types. It is frequent in AL type (immunoglobulin light chain derived) and ATTR type (transthyretin derived) but infrequent in AA type (serum amyloid A protein derived) amyloidosis (Falk et al. 1997; Sipe et al. 2012). Cardiac involvement eventually leads to a type of cardiomyopathy that does not present with ventricular hypertrophy or dilatation. Instead, it leads to restricted ventricular filling, resulting in symptoms and signs of heart failure. Heart failure occurs in at least 25 % of all patients (Dubrey et al. 1998). In ATTR amyloidosis, however, cardiac involvement initially leads less frequently to systolic dysfunction and heart failure. Furthermore, symptoms are milder and progression is slower, when

compared to AL amyloidosis. Restrictions in ventricular filling result in persistently elevated venous pressures, liver enlargement, ascites and oedema, i.e. the clinical picture of right-sided heart failure. Consequently, patients usually suffer from dyspnoea and fatigue. Amyloidosis is the most common cause of this so-called restrictive cardiomyopathy.

The diagnosis is based on histological proof from endomyocardial biopsy, especially when amyloidosis is limited to the heart. Four samples provide a sensitivity of nearly 100 %, and a negative biopsy almost always rules out the disease. But this gold standard is not met in most patients, because the diagnosis is very likely when amyloid has been detected in extra-cardiac tissue (e.g. in subcutaneous abdominal fat tissue, see Fig. 16.1) in combination with the typical clinical picture of amyloid cardiomyopathy (Gertz et al. 2005). Since endomyocardial biopsy harbours a risk in these patients, a non-invasive diagnostic tool is clinically valuable. Different imaging modalities are used for haemodynamics and determination of prognosis. Correct and early recognition of cardiac amyloidosis and its various types remains a challenge.

The prognosis of cardiac amyloidosis is worse compared to other manifestations of the disease. Cardiac AL amyloidosis is often rapidly progressive, and, in patients with ventricular septum thickness >15 mm, left ventricular ejection fraction (LVEF) <40 % and symptoms of heart failure, the median survival is less than 6 months (Ronsyn et al. 2011). No specific treatment exists for cardiac amyloidosis or restrictive cardiomyopathy. However, heart failure should be treated with diuretics, and cardiac transplantation might be considered in selected cases. Early detection of cardiac involvement is essential as the presence and severity of cardiac amyloidosis clearly influence the treatment options to stop progression of the disease and, even more importantly, directly affect prognosis.

16.1.1 The Role of Non-scintigraphic Imaging Modalities

A detailed outline on the role of non-scintigraphic imaging modalities to assess potential cardiac amyloidosis is not in the scope of this book chapter. In short, transthoracic echocardiography and cardiac magnetic resonance imaging with gadolinium enhancement are discussed.

Transthoracic echocardiography plays an important role in the evaluation of cardiac manifestation of amyloidosis. Nowadays, it is the modality of choice for the evaluation of amyloid deposition in the heart (Falk et al. 1987). The most common finding is left ventricular wall thickening due to amyloid deposition in the myocardium. This is often associated with right ventricular wall thickening, diffuse valvular infiltration, dilated atria and pericardial effusion (Klein et al. 1990). Although echocardiography plays a major role, the diagnosis of cardiac amyloidosis is often only possible when the disease has reached an advanced stage, where irreversible functional and structural myocardial changes have occurred. There is an obvious need for methods that detect cardiac amyloidosis in an earlier and preferentially presymptomatic phase.

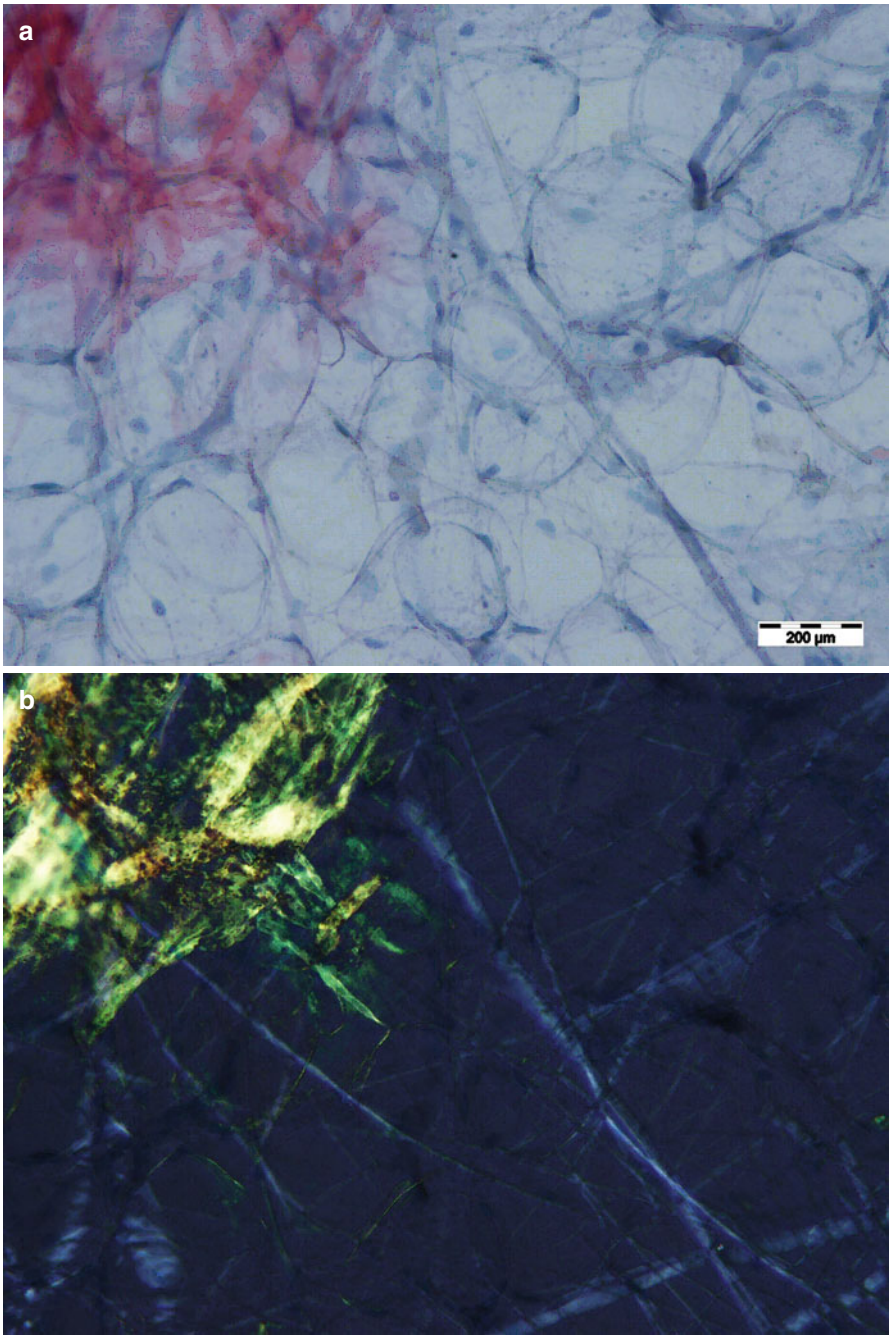

Fig. 16.1 An example of an abdominal subcutaneous fat aspirate exposing amyloid deposits, stained with Congo red. (**a**) Viewed in normal light: amyloid is stained red. Bar length is 200 µm. (**b**) Viewed in polarised light: amyloid shows apple-green birefringence (collagen is bluish white)

If echocardiography is inconclusive, cardiac magnetic resonance imaging with gadolinium enhancement might be useful. Gadolinium is an extracellular fluid tracer which accumulates in expanded interstitial place. Usually, in the intact myocardium, the distribution of gadolinium is very low, and therefore gadolinium enhancement is absent. However, in the case of myocardial interstitial space expansion, such as in amyloidosis due to extracellular amyloid infiltration, gadolinium concentration may increase within myocardial tissue. Global subendocardial late gadolinium enhancement can be found in approximately two-thirds of patients with systemic amyloidosis (Maceira et al. 2005). However, the value of MRI for the early detection of cardiac involvement is not clear.

16.1.2 The Role of Scintigraphic Imaging Modalities

Scintigraphy, using labelled serum amyloid P component (SAP), provides not only information on different organ distributions, but serial scans can provide evidence of progression and regression of the disease (Hawkins 2002). Unfortunately, these SAP scans are unsuitable for detecting amyloid deposition in the myocardium, due to size of the tracer, heart movement, blood-pool content and residual tracer uptake in the spleen.

Autonomic innervation abnormalities resulting in impaired gastric emptying is fairly common in patients with hereditary ATTR amyloidosis, in which disease a TTR mutation causes amyloid deposition (Wixner et al. 2012). Scintigraphic gastric emptying studies can play a role in identifying gastric retention due to ATTR amyloidosis. This same modality had been used to evaluate the effect of liver transplantation on gastric emptying. It showed that liver transplantation eventually had no effect on the gastric emptying time in these patients (Suhr et al. 2003).

Myocardial adrenergic denervation, using iodine-123 meta-iodobenzylguanidine ([^{123}I]-MIBG), has been shown present in patients with amyloidosis (Nakata et al. 1995; Tanaka et al. 1997; Delahaye et al. 1999). Indirectly, [^{123}I]-MIBG visualises the effect of amyloid deposition in the myocardium. This technique might be able to detect early cardiac denervation before ongoing deposition of amyloid leads to actual heart failure. Table 16.1 provides an overview of the diagnostic criteria for the assessment of cardiac amyloidosis, using the above-mentioned imaging modalities. The purpose of this book chapter is to discuss the role of [^{123}I]-MIBG in the assessment of cardiac amyloidosis.

16.2 Consequences of Impaired Sympathetic Innervation in Cardiac Amyloidosis

Cardiac amyloidosis is a form of restrictive cardiomyopathy, due to the progressive deposition of amyloid fibrils in myocardium and direct depression of diastolic function. Usually this occurs in both left and right ventricles, causing biventricular heart failure. But cardiac amyloidosis often presents itself as severe right-sided heart failure only. Eventually, systolic dysfunction leads to congestive heart failure. This

Table 16.1 Diagnostic criteria for cardiac amyloidosis

Imaging modality	Findings in cardiac amyloidosis	Remarks
Endomyocardial biopsy	Positive Congo red staining	Gold standard, however invasive method
Transthoracic echocardiography	Main findings:	Modality of choice, however often only positive in advanced stage of disease
	Left ventricular wall thickening	
	Highly refractile (sparkling cardiac echoes)	
	Associated findings:	
	Right ventricular wall thickening	
	Diffuse valvular infiltration	
	Dilated atria	
	Pericardial effusion	
Magnetic resonance imaging	Global subendocardial late gadolinium enhancement	Aspecific finding. No role in early stage of disease
[^{123}I]-MIBG scintigraphy	Planar views:	Restricted to AL and ATTR patients. Positive test results before abnormalities on echocardiography
	Low heart-to-mediastinum ratio (HMR, <1.6) at 4 h post injection	However, inferior wall defect on SPECT can be false positive
	High wash-out rate (>20 %) at 4 h post injection	
	SPECT:	
	Segmental defect on polar map view	

occurs only in late stages because the left ventricular ejection fraction (LVEF) remains (nearly) normal until late in disease. Symptoms caused by heart failure are dyspnoea, orthopnoea, peripheral oedema and sometimes, in late stages of the disease, ascites.

Amyloid deposition in the atria can cause atrial fibrillation (AF) that causes complaints of fast and irregular heart action. Also, AF is associated with the development of thromboembolism. A poor LVEF and amyloid infiltration can contribute to the complications of embolisms (e.g. cerebral infarction).

Furthermore, microvascular disease does not only cause complaints of angina due to myocardial ischemia (Mueller et al. 2000), it also often leads to syncope (Chamarthi et al. 1997). The development of syncope seems to be based on multiple

factors. First, it may be a consequence of bradycardia due to amyloid infiltration in the conduction system. Secondly, a syncope can be a result of sustained ventricular tachycardia. Third, it may be caused by hypotension due to autonomic neuropathy or forward failure, sometimes aggravated by overuse of diuretic drugs. Finally, it may be the onset of sudden cardiac death due to electromechanical dissociation rather than ventricular dysrhythmias (Falk et al. 1984).

16.3 Use of Planar Images of [^{123}I]-MIBG in Amyloidosis

The use of [^{123}I]-MIBG is studied most intensively in patients with hereditary ATTR amyloidosis with polyneuropathy, formerly called familial amyloidotic polyneuropathy. The first reported case of severe peripheral neuropathy due to hereditary ATTR, in which 111 MBq [^{123}I]-MIBG was used, did not show any definite myocardial activity in all cardiac regions on either early (30 min post injection (pi)) or late images (4 h pi) (Nakata et al. 1995); see also an example of a normal and abnormal [^{123}I]-MIBG scan in Figs. 16.2 and 16.3. Although the cardiac walls were markedly thickened by amyloid, the left ventricular ejection fraction was normal on radionuclide ventriculography, as well as myocardial perfusion using thallium-201 ([^{201}Tl]). Analysis of heart rate variability (HRV) suggested highly damaged vagal and sympathetic activities. Thus, the defects on the [^{123}I]-MIBG scan were considered to represent impaired sympathetic nerve endings in the heart due to amyloid deposition.

The lack of [^{123}I]-MIBG uptake in myocardial tissue was also seen in a second case report (Arbab et al. 1997). In this patient with hereditary ATTR, a [^{123}I]-MIBG scan was performed, which showed no uptake in the heart, indicating severe impairment of cardiac sympathetic function. Also several other investigations were performed, including technetium-99m-labelled dimercaptosuccinic acid ([^{99m}Tc]-DMSA),

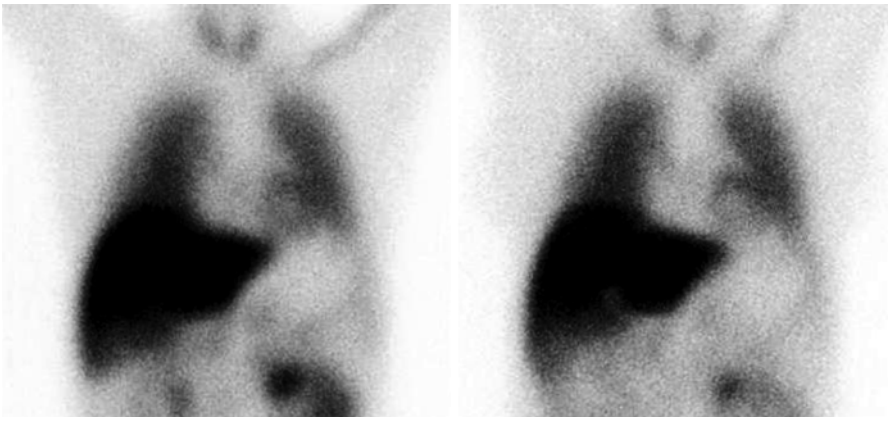

Fig. 16.2 An example of normal [^{123}I]-MIBG uptake. HMR on early (*left*) image 2.50, HMR on late (*right*) image 2.50, wash-out 0 %

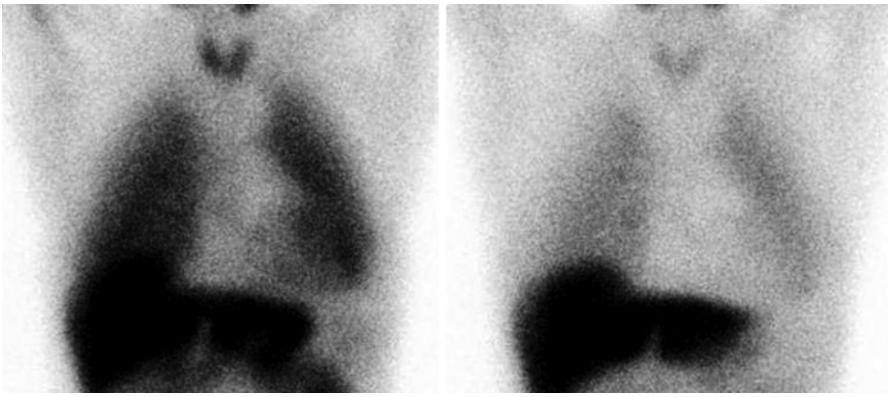

Fig. 16.3 An example of abnormal [^{123}I]-MIBG uptake in a patient with amyloid deposition. HMR on early (*left*) image 1.89, HMR on late (*right*) image 1.37, wash-out 27 %

[^{201}Tl] and iodine-123-labelled 15-(p-iodophenyl)-3-(R,S)-methyl-pentadecanoic acid ([^{123}I]-BMIPP) studies. These studies showed myocardial involvement of amyloidosis ([^{99m}Tc]-DMSA), normal myocardial perfusion ([^{201}Tl]) and normal fatty acid metabolism ([^{123}I]-BMIPP), respectively.

In the first clinical study, 12 patients with hereditary ATTR and polyneuropathy were prospectively followed, using [^{123}I]-MIBG and comparing it to echocardiography, and to [^{201}Tl] and [^{99m}Tc]-labelled pyrophosphate ([^{99m}Tc]-PYP) imaging studies (Tanaka et al. 1997). All 12 patients suffered from biopsy-proven cardiac amyloidosis. Four mCi (148 MBq) [^{123}I]-MIBG was administered and scans were performed 30 min and 3 h post injection (pi). In 8 out of these 12 patients no myocardial uptake of [^{123}I]-MIBG was found on either the early or the late images. The remaining four patients showed only limited uptake in the anterior wall on both early and late images. Four patients had left ventricle (LV) wall thickening on echocardiography, with otherwise normal results. There was no significant correlation found between the prevalence of decreased uptake of [^{123}I]-MIBG and LV wall thickness and results of [^{99m}Tc]-PYP scans. All 12 patients had normal myocardial perfusion on [^{201}Tl] scan. So, in conclusion, patients with hereditary ATTR amyloidosis and polyneuropathy were found to have a high incidence of myocardial adrenergic denervation with viable myocardium, which can be found early in cardiac amyloidosis in the absence of clinically apparent heart disease.

In the second clinical study, 17 patients with hereditary ATTR amyloidosis and polyneuropathy were analysed before liver transplantation (Delahaye et al. 1999). All patients had biopsy-proven ATTR amyloid by specimens from either rectal mucosa or peripheral nerves. These patients underwent [^{123}I]-MIBG (300 MBq) scanning at 20 min and 4 h pi, heart rate variability analysis, coronary angiography, radionuclide ventriculography, rest [^{201}Tl] scan, echocardiography and measurement of plasma catecholamine levels. [^{123}I]-MIBG scans were also performed in 12 age-matched control subjects. Planar [^{123}I]-MIBG images were analysed using

HMR and wash-out rate, defined as percent change in activity from early to late images within the LV. No patients showed evidence of coronary artery disease, perfusion defects or diminished LVEF. However, cardiac [^{123}I]-MIBG uptake was dramatically decreased in ATTR patients compared to the age-matched control population, on both early and late images (HMR at 4 h: 1.36 ± 0.26 vs. 1.98 ± 0.35, $p < 0.001$). The wash-out rate was not significantly different. On the other hand, cardiac [^{123}I]-MIBG uptake at 4 h correlated with the severity of polyneuropathy. In concordance to the results of the former mentioned study, these patients with ATTR amyloidosis had sympathetic denervation as assessed by [^{123}I]-MIBG imaging, despite normal LV systolic function and myocardial perfusion.

In continuation of these findings a subsequent study in 31 patients with hereditary ATTR amyloidosis and polyneuropathy was performed after liver transplantation (Delahaye et al. 2006). The purpose of this study was to evaluate the outcomes of cardiac sympathetic innervation and amyloid infiltration after liver transplantation. Cardiac sympathetic innervation was assessed in the same manner as the study published in 1999 by the same authors: 300 MBq [^{123}I]-MIBG, scans at 20 min and 4 h pi and the use of HMR and wash-out rates. A similar age-matched control population was used for normal values of HMR and wash-out rate. All patients also underwent a [^{201}Tl] scan at rest, heart rate variability analysis, echocardiography, and right heart catheterisation. Sympathetic denervation was found in patients before liver transplantation compared to the control population (HMR 1.45 ± 0.29 vs. 1.98 ± 0.35, $p < 0.001$) After liver transplantation, there was no significant change in global [^{123}I]-MIBG HMR (1.46 ± 0.28). This may implicate that progression of cardiac sympathetic denervation stops after liver transplantation and that early reinnervation cannot be measured within 2 years after liver transplantation. There was no correlation found between age and echocardiographic findings. However, conduction disturbances, ventricular arrhythmias and LV wall thickening were associated with low [^{123}I]-MIBG uptake and progressed after liver transplantation. This may implicate progression of cardiac amyloid infiltration after liver transplantation (Haagsma et al. 2007). Low cardiac [^{123}I]-MIBG uptake was also in this study associated with severity of polyneuropathy, which worsened after liver transplantation. The authors conclude that [^{123}I]-MIBG imaging can provide an objective measurement of cardiac sympathetic innervation, which could help to guide the indications for liver transplantation in patients with early stage of hereditary ATTR amyloidosis and polyneuropathy.

Although symptoms and consequences of cardiac amyloid deposition in AL amyloidosis are often more frequent and severe than in ATTR amyloidosis (causing more frequently fatal dysfunction), the use of [^{123}I]-MIBG in this type of disease has hardly been studied. In fact only one major study has been performed in which the presence of impaired myocardial sympathetic innervation was related to clinical autonomic abnormalities and congestive heart failure in AL amyloidosis (Hongo et al. 2002). In this study 25 patients with biopsy-proven cardiac manifestation of AL amyloidosis underwent autonomic function tests, echocardiography, heart rate variability analysis and [^{123}I]-MIBG scanning. The [^{123}I]-MIBG scans were performed using 111 MBq [^{123}I]-MIBG with uptake at 30 min and 3 h pi. Myocardial

uptake and wash-out rates were calculated using HMR. Furthermore, 20 of 25 patients underwent [^{201}Tl] scan at rest for myocardial perfusion. Of the 25 patients, 9 suffered from autonomic dysfunction and 16 did not. Five of 9 patients with autonomic dysfunction and 10 of 16 without had congestive heart failure. Between the two groups with and without autonomic dysfunction, no significant difference was found in amyloid deposition in the right and left ventricular wall based on echocardiographic thickness. None of the patients had myocardial perfusion defects. In patients with autonomic dysfunction, HMR (1.37 ± 0.05 vs. 1.66 ± 0.09 after 30 min, $p < 0.001$, and 1.29 ± 0.05 vs. 1.53 ± 0.06 after 3 h, $p < 0.001$) and wash-out rates (30.8 ± 4.0 % vs. 41.5 ± 4.8 %) were significantly decreased compared to the patients without autonomic dysfunction. In both groups, HMR was significantly decreased and wash-out rate increased in patients with heart failure (10 of 16 without autonomic dysfunction, 5 of 9 with autonomic symptoms) compared to the patients without heart failure. Therefore, myocardial uptake and turnover of [^{123}I]-MIBG in patients with AL amyloidosis are heterogeneous and seem to depend on the presence of both congestive heart failure and cardiac autonomic dysfunction.

In the most recent study, 61 patients with biopsy-proven amyloidosis (39 AL, 11 AA, 11 ATTR) underwent general clinical work-up, echocardiography and [^{123}I]-MIBG scintigraphy (Noordzij et al. 2012). Using echocardiography, left ventricular internal dimensions and wall thickness were measured, and highly refractile ('sparkling') cardiac echoes were assessed. These findings were compared with the early (15 min) and late (4 h) HMR and wash-out rates, determined after administration of [^{123}I]-MIBG. The echocardiographic parameters did not significantly differ among the three patient groups. Sparkling was present in 72 % of ATTR patients, in 54 % of AL patients and in 45 % of AA patients. Mean late HMR in all patients was 2.3 ± 0.75, and the mean wash-out rate was 8.6 ± 14 % (the latter did not significantly differ among the patient groups). Late HMR was significantly lower in patients with echocardiographic signs of amyloidosis than in patients without (2.0 ± 0.70 vs. 2.8 ± 0.58, $p < 0.001$). Also, wash-out rates were significantly higher in these patients (17 ± 10 % vs. -3.3 ± 9.9 %, $p < 0.001$). Furthermore, in ATTR patients with polyneuropathy but without echocardiographic signs of amyloidosis, HMR was lower than in patients with other types of amyloidosis (2.0 ± 0.59 vs. 2.9 ± 0.50, $p = 0.007$).

So, in conclusion, this study confirms that [^{123}I]-MIBG HMR is lower and wash-out rate is higher in patients with echocardiographic signs of amyloidosis. Also, [^{123}I]-MIBG scintigraphy is able to detect cardiac denervation in ATTR patients before signs of amyloidosis are evident on echocardiography.

16.4 Discussion

Amyloidoses are systemic diseases that affect multiple organs and tissues and carry a poor prognosis. The need to identify cardiac involvement is very urgent, because of high rates of arrhythmia, rapid deterioration and sudden cardiac death. Diagnostic imaging is important for risk assessment and decision making concerning drug

treatment, liver transplantation, Implantable Cardioverter Defibrillator (ICD) implants and heart transplantation. This book chapter focuses on the use of [^{123}I]-MIBG, being the best literature-based imaging modality for cardiac sympathetic denervation. Myocardial defects in [^{123}I]-MIBG activity correlate with impaired cardiac sympathetic function due to amyloid deposition. This can be identified early in the disease. Furthermore, lower HMR and higher wash-out rates correspond to severity of the disease.

The use of HMR and wash-out rates have also been used in patients with other forms of heart failure. These studies have shown that decreased HMR on late images and increased wash-out rates are related to an increase in systolic dysfunction. Lower [^{123}I]-MIBG uptake was even reported to indicate poorer prognosis in patients with heart failure. In the recently published ADMIRE-HF (AdreView Myocardial for Risk Evaluation in Heart Failure, AdreView = [^{123}I]-MIBG) study, 961 patients with NYHA (New York Heart Association) functional class II/III and LVEF $\leq$ 35 % were followed for 2 years. All underwent [^{123}I]-MIBG (early and late) and myocardial perfusion imaging. The primary goal was to relate HMR <1.60 to a composite end point, including progression of NYHA functional class (worsening of heart failure), potentially life-threatening arrhythmic event or cardiac death. The cumulative 2-year event rate of the composite end point was significantly lower in patients with HMR $\geq$1.60 (15 % vs. 38 %, $p < 0.001$) (Jacobson et al. 2010). Imaging with [^{123}I]-MIBG seemed to be of independent prognostic value in patients with heart failure. In a subsequent multivariate analysis, HMR was reported to be an independent predictor of both cardiac and all-cause death (Travin et al. 2009). Surprisingly, this multivariate analysis showed that diabetes was no independent predictor. Patients with diabetes are considered to develop autonomic neuropathy during their life. However, another group did show that patients with diabetes, without clinical symptoms of myocardial ischemia, had low HMR and high wash-out (Scholte et al. 2010). [^{123}I]-MIBG scintigraphy even identified autonomic neuropathy in more patients than sequential performed heart rate variety analysis. Furthermore, in the past it was already shown that HMR of patients with diabetes was lower than healthy control subjects (Langer et al. 1995). This may indicate that in patients with amyloidosis, diabetes may play a confounding role.

As mentioned before, normal values for HMR and wash-out rates seem to vary, not only among different ages but also among different image acquisitions protocols. Concerning the image acquisition, the most important factor seems to be the collimator used for [^{123}I]-MIBG imaging. In addition to the 159 keV peak which is used for imaging, [^{123}I]-MIBG also has a 529 keV peak. Collimators exhibit different degree of scattering by gamma rays of 529 keV, so that these rays mix in with the data from 159 keV rays. The image quality is impaired by these scattered rays, when using low-energy collimators. A medium energy collimator seems to solve this problem, although not every institution will have access to such a collimator (Verberne et al. 2005; Dobbeleir et al. 1999; Inoue et al. 2003). Other factors causing differences in HMR and wash-out rates are the methods of setting regions of interest (ROIs) (especially concerning site, size and form), the moment of late images, the duration of an acquisition and the correction for decay (Yamashino and Yamazaki 2007; Verberne

et al. 2008). On the other hand, according to blood activity, the slope of vascular clearance curves or estimated renal function (eGFR), variations in the quantity of vascular structures in the mediastinum and the rate of renal clearance of [^{123}I]-MIBG from the blood pool do not seem to contribute to increased inter individual variation in uptake on either early or late images (Verberne et al. 2011). In a recent proposal to standardise [^{123}I]-MIBG cardiac sympathetic imaging, evidence-based recommendations for, among others, image acquisition, collimator choice and data analysis are enlisted for routine clinical application. Standardisation of [^{123}I]-MIBG cardiac imaging should contribute to its clinical applicability and integration into current nuclear cardiology practice (Verberne et al. 2008; Flotats et al. 2010).

16.4.1 Single-Photon Emission Computed Tomography (SPECT)

The focus of this book chapter was the role of planar images of [^{123}I]-MIBG in cardiac amyloidosis and their place in the evaluation of cardiac sympathetic function. The acquisition of SPECT has also been reported and has advantages for evaluating abnormalities in regional distribution in the myocardium (Nakata et al. 1995; Tanaka et al. 1997; Delahaye et al. 1999, 2006; Arbab et al. 1997; Hongo et al. 2002). Usually, the reconstructed data are displayed in three planes (short axis, horizontal long axis and vertical long axis), which is similar to that used in myocardial perfusion SPECT. Various distribution patterns of myocardial [^{123}I]-MIBG accumulation have been reported. In 16 patients with AL amyloidosis who had no autonomic dysfunction, only two had a homogeneous distribution of [^{123}I]-MIBG (Hongo et al. 2002). The reduced uptake in the other patients was mainly localised in inferior and inferoposterior wall segments. Of the nine patients with autonomic dysfunction, five had only [^{123}I]-MIBG accumulation in the anterior wall. The reduced uptake and focal defects in the inferior wall were also reported in the ATTR patients studied before liver transplantation (Delahaye et al. 1999). These inferior wall defects should be interpreted carefully, hence substantial [^{123}I]-MIBG uptake in the liver may overlap the myocardial inferoposterior wall. In addition, even in normal cases, [^{123}I]-MIBG uptake is relatively low in the inferior wall, especially in the elderly (Gill et al. 1993; Estorch et al. 1995; Tsuchimochi et al. 1995).

Analogue to myocardial perfusion imaging, the use of polar maps can be used to calculate extent and severity scores for segmental defects. Comparing perfusion imaging to [^{123}I]-MIBG distribution provides extra information about the presence or absence of mismatch patterns. Myocardial ischemia or infarction disrupts sympathetic transmission, which may lead to denervation of a region larger than affected by ischemia only. Furthermore, sympathetic nervous tissue is more sensitive to ischemia than cardiomyocytes. The presence of innervation/perfusion imaging mismatches correlates with electrophysiological abnormalities and increasing inducibility of potential lethal dysrhythmia (Simoes et al. 2004; Sasano et al. 2008).

16.4.2 Future Perspectives

Various positron emission tomography (PET) analogues of norepinephrine are evaluated in heart diseases (Bengel and Schwaiger 2004). These PET tracers even show more similarities to norepinephrine than [^{123}I]-MIBG and bear several advantages for imaging. [^{11}C]-meta-hydroxy-ephedrine ([^{11}C]-mHED) is the most commonly used PET tracer. It has a higher sensitivity for the uptake-1 mechanism than [^{123}I]-MIBG and is not influenced by the uptake-2 mechanism, which might implicate a better differentiation between innervated and denervated myocardium. In a group of 21 patients with left ventricular dysfunction who underwent both [^{123}I]-MIBG and [^{11}C]-mHED imaging, the correlation between [^{123}I]-MIBG wash-out rate and mHED wash-out rate was poor ($r = 0.57$). But the defect size on both early ($r = 0.94$) and late images ($r = 0.88$) was more closely related between these two modalities. [^{11}C]-mHED seems to have advantages over [^{123}I]-MIBG in regional abnormalities (Matsunari et al. 2010). Other [^{11}C]-labelled tracers like [^{11}C]-phenethylguanidine are currently under investigation. Promising results from a study using rats show that [^{11}C]-phenethylguanidine and its analogues are transported slower than MIBG and mHED and therefore might provide a more accurate measurement of cardiac nerve activation (Raffel et al. 2007). Finally, a fluorine-18 ([^{18}F])-labelled PET tracer has been developed: N-[3-Bromo-4-(3-[^{18}F]fluoro-propoxy)-benzyl]-guanidine (LMI1195), which is a norepinephrine transporter substrate (Yu et al. 2011). In rats, the uptake of LM1195 in the heart appeared to be similar to [^{123}I]-MIBG, whereas the heart-to-lung ratios were significantly higher. Chemical cardiac sympathetic denervation resulted in a decrease in cardiac LM1195 uptake.

We are not aware that PET tracers already have been used to visualise cardiac denervation in patients with cardiac manifestation of amyloidosis.

Conclusions

The use of [^{123}I]-MIBG in cardiac sympathetic denervation is well established. Several studies point out the value of HMR and wash-out rate as parameters for sympathetic innervation abnormalities in cardiac amyloidosis. The method is highly reproducible and easily accessible, thereby making substitution by other modalities less attractive. However, there is an increasing urge to standardise quantitative values, such as HMR and wash-out rate.

References

Arbab AS, Koizumi K, Toyama K et al (1997) Scan findings of various myocardial SPECT agents in a case of amyloid polyneuropathy with suspected myocardial involvement. Ann Nucl Med 11:139–141

Bengel FM, Schwaiger M (2004) Assessment of cardiac sympathetic neuronal function using PET imaging. J Nucl Cardiol 11:603–616

Chamarthi B, Dubrey SW, Cha K et al (1997) Features and prognosis of exertional syncope in light-chain associated AL cardiac amyloidosis. Am J Cardiol 80:1242–1245

Delahaye N, Dinanian S, Slama MS et al (1999) Cardiac sympathetic denervation in familial amyloid polyneuropathy assessed by iodine-123 metaiodobenzylguanidine scintigraphy and heart rate variability. Eur J Nucl Med 26:416–424

Delahaye N, Rouzet F, Sarda L et al (2006) Impact of liver transplantation on cardiac autonomic denervation in familial amyloid polyneuropathy. Medicine 85:229–238

Dobbeleir AA, Hambye AS, Franken PR (1999) Influence of high energy photons on the spectrum of iodine-123 with low- and medium-energy collimators: consequences for imaging with 123I labelled compounds in clinical practice. Eur J Nucl Med 26:655–658

Dubrey SW, Cha K, Anderson J et al (1998) The clinical features of immunoglobulin light-chain (AL) amyloidosis with heart involvement. QJM 91:141–157

Estorch M, Carrio I, Berna L et al (1995) Myocardial iodine-labeled metaiodobenzylguanidine 123 uptake relates to age. J Nucl Cardiol 2:126–132

Falk RH, Rubinow A, Cohen AS (1984) Cardiac arrhythmias in systemic amyloidosis: correlation with echocardiographic abnormalities. J Am Coll Cardiol 3:107–113

Falk RH, Plehn J, Deering T et al (1987) Sensitivity and specificity of the echocardiographic features of cardiac amyloidosis. Am J Cardiol 59:418–422

Falk RH, Comenzo RL, Skinner M (1997) The systemic amyloidosis. N Engl J Med 337: 898–909

Flotats A, Carrió I, Agostini D et al (2010) Proposal for standardization of 123I-metaiodobenzylguanidine (MIBG) cardiac sympathetic imaging by the EANM Cardiovascular Committee and the European Council of Nuclear Cardiology. Eur J Nucl Med Mol Imaging 37:1802–1812

Gertz MA, Comenzo R, Falk RH et al (2005) Definition of organ involvement and treatment response in immunoglobulin light chain amyloidosis (AL): a consensus opinion from the 10th International Symposium on Amyloid and Amyloidosis. Am J Hematol 79:319–328

Gill JS, Hunter GJ, Gane G et al (1993) Heterogeneity of the human myocardial sympathetic innervation: in vivo demonstration by iodine 123-labeled meta-iodobenzylguanidine scintigraphy. Am Heart J 126:390–398

Haagsma EB, van Gameren II, Bijzet J et al (2007) Familial amyloidotic polyneuropathy: long-term follow-up of abdominal fat tissue aspirate in patients with and without liver transplantation. Amyloid 14:221–226

Hawkins PN (2002) Serum amyloid P component scintigraphy for diagnosis and monitoring amyloidosis. Curr Opin Nephrol Hypertens 11:649–655

Hongo M, Urushibata K, Kai R et al (2002) Iodine-123 metaiodobenzylguanidine scintigraphic analysis of myocardial sympathetic innervation in patients with AL (primary) amyloidosis. Am Heart J 144:122–129

Inoue Y, Suzuki A, Shirouzu I et al (2003) Effect of collimator choice on quantitative assessment of cardiac iodine 123 MIBG uptake. J Nucl Cardiol 10:623–632

Jacobson AF, Senior R, Cerqueira MD et al (2010) Myocardial iodine-123 meta-iodobenzylguanidine imaging and cardiac events in heart failure: Results of the prospective ADMIRE-HF (AdreView myocardial imaging for risk evaluation in heart failure) study. J Am Coll Cardiol 55: 2212–2221

Klein AL, Hatle LK, Taliercio CP et al (1990) Serial Doppler echocardiographic follow-up of left ventricular diastolic function in cardiac amyloidosis. J Am Coll Cardiol 16:1135–1141

Langer A, Freeman MR, Josse RG et al (1995) Metaiodobenzylguanidine imaging in diabetes mellitus: assessment of cardiac sympathetic denervation and its relation to autonomic dysfunction and silent myocardial ischemia. J Am Coll Cardiol 25:610–618

Maceira AM, Joshi J, Prasad SK et al (2005) Cardiovascular magnetic resonance in cardiac amyloidosis. Circulation 111:186–193

Matsunari I, Aoki H, Nomura Y et al (2010) Iodine-123 metaiodobenzylguanidine imaging and carbon-11 hydroxyephedrine positron emission tomography compared in patients with left ventricular dysfunction. Circ Cardiovasc Imaging 3:595–603

Mueller PS, Edwards WD, Gertz MA (2000) Symptomatic ischemic heart disease resulting from obstructive intramural coronary amyloidosis. Am J Med 109:181–188

Nakata T, Shimamoto K, Yonekura S et al (1995) Cardiac sympathetic denervation in transthyretin-related familial amyloidotic polyneuropathy: detection with iodine-12-MIBG. J Nucl Med 36:1040–1042

Noordzij W, Glaudemans AW, van Rheenen RWJ et al (2012) (123)I-Labelled metaiodobenzylguanidine for the evaluation of cardiac sympathetic denervation in early stage amyloidosis. Eur J Nucl Med Mol Imaging 39:1609–1617

Raffel DM, Jung YW, Gildersleeve DL et al (2007) Radiolabeled phenethylguanidines: novel imaging agents for cardiac sympathetic neurons and adrenergic tumors. J Med Chem 50: 2078–2088

Ronsyn M, Shivalkar B, Vrints CJM (2011) Cardiac amyloidosis in full glory. Heart 97:720

Sasano T, Abraham R, Chang KC et al (2008) Abnormal sympathetic innervation of viable myocardium and the substrate of ventricular tachycardia after myocardial infarction. J Am Coll Cardiol 51:2266–2275

Scholte AJHA, Schuijf JD, Delgado V et al (2010) Cardiac autonomic neuropathy in patients with diabetes and no symptoms of coronary artery disease: comparison of ^{123}I-metaiodobenzylguanidine myocardial scintigraphy and heart rate variability. Eur J Nucl Med Mol Imaging 37:1698–1705

Simões MV, Barthel P, Matsunari I et al (2004) Presence of sympathetically denervated but viable myocardium and its electrophysiologic correlates after early revascularised, acute myocardial infarction. Eur Heart J 25:551–557

Sipe JD, Benson MD, Buxbaum JN et al (2012) Amyloid fibril protein nomenclature: 2012 recommendations from the Nomenclature Committee of the International Society of Amyloidosis. Amyloid 19:167–170

Suhr OB, Anan I, Ahlström KR et al (2003) Gastric emptying before and after liver transplantation for familial amyloidotic polyneuropathy, Portuguese type (Val30Met). Amyloid 10:121–126

Tanaka M, Hongo M, Kinoshita O et al (1997) Iodine-123 metaiodobenzylguanidine scintigraphic assessment of myocardial sympathetic innervation in patients with familial amyloid polyneuropathy. J Am Coll Cardiol 29:168–174

Travin M, Anathassubramaniam K, Henzlova MJ et al (2009) Imaging of myocardial sympathetic innervation for prediction of cardiac and all-cause mortality in heart failure: analysis from the ADMIRE-HF trial. Circulation 120:S350

Tsuchimochi S, Tamaki N, Tadamura E et al (1995) Age and gender differences in normal myocardial adrenergic neuronal function evaluated by iodine-123-MIBG imaging. J Nucl Med 36: 969–974

Verberne HJ, Feenstra C, de Jong WM et al (2005) Influence of collimator choice and simulated clinical conditions on 123I-MIBG heart/mediastinum ratios: a phantom study. Eur J Nucl Med Mol Imaging 32:1100–1107

Verberne HJ, Habraken JB, van Eck-Smit BL et al (2008) Variations in 123I-metaiodobenzylguanidine (MIBG) late heart mediastinal ratios in chronic heart failure: a need for standardisation and validation. Eur J Nucl Med Mol Imaging 35:547–553

Verberne HJ, Verschure DO, Somsen GA et al (2011) Vascular time-activity variation in patients undergoing ^{123}I-MIBG myocardial scintigraphy: implications for quantification of cardiac and mediastinal uptake. Eur J Nucl Med Mol Imaging 38:1132–1138

Wixner J, Karling P, Rydh A et al (2012) Gastric emptying in hereditary transthyretin amyloidosis: the impact of autonomic neuropathy. Neurogastroenterol Motil 24:1111–e568

Yamashino S, Yamazaki J (2007) Neuronal imaging using SPECT. Eur J Nucl Med Mol Imaging 34:S62–S73

Yu M, Bozek J, Lamoy M et al (2011) Evaluation of LMI1195, a novel 18F-labeled cardiac neuronal PET imaging agent, in cells and animal models. Circ Cardiovasc Imaging 4:435–443